ORIGINAL PAPER

A robust fuzzy speed regulator for unmanned sailboat robot via the composite ILOS guidance

Guoqing Zhang · **Jiqiang Li** · **Cheng Liu** · **Weidong Zhang**

Abstract This note deals with the waypoints-based path following control problem for the unmanned sailboat robot (USR), aiming to obtain the speed controllable performance and tackle with the constraints of the unknown environment disturbances and the model uncertainties. For this purpose, the composite integral line-of-sight guidance principle is targetedly designed for the upwind, the downwind and the crosswind cases to generate the real time heading reference for the USR. For the control part, the robust fuzzy speed regulator and the heading controller are proposed by fusing the dynamic surface control and the robust fuzzy damping technique. The corresponding control inputs are the sail angle and the rudder angle, respectively. In the proposed scheme, the model unknown terms and the gain uncertainties are tackled, and there are only two adaptive parameters to be updated online. Especially, the speed controllable performance of USR is significant and meaningful for the practical path following mission. That can guarantee or enhance the stabilization of the closed-loop control system. Sufficient effort has been made to guarantee the semi-global uniform ultimate bounded stability via the Lyapunov theory. Through simulation verification, the pro- posed approach can obtain the satisfied heading tracking accuracy and speed regulating performance.

1 Introduction

In recent years, more advanced automatic control scheme is prevailing in the field of underactuated surface vehicles, except for the traditional autopilot system. The sailboat control is a class of significant application in the marine engineering, such as ocean investigation, exploitation, and surveillance mission [1,2]. The unmanned sailboat robot (USR) can undertake the long-range and long-term oceanic monitoring missions for its merits of relying on the renewable energy, i.e. wind energy [3]. However, since it is required to steer the rudder along with the specific heading angle and adjust the sail to obtain the propulsion simultaneously, the various marine environment and the specific waypoints-based path may cause the instability or invalidation of the closed-loop system. At the same time, one of the main attention of the researchers is to get the adequate surge velocity towards the desired direction by adjusting the sail angle [4]. To improve the effectiveness and the speed performance of path following in the complex missions, the intelligent guidance and control scheme for the USR should be further

G. Zhang (✉) · J. Li. C.Liu
Navigation College, Dalian Maritime University, Dalian 116026, Liaoning, People's Republic of China
e-mail: zgq_dlmu@163.com

W. Zhang
Department of Automation, Shanghai Jiao Tong University, Shanghai 200240, People's Republic of China

investigated and are meaningful for the practical engineering.

The sailboat control has been becoming a hotspot topic for its merits of green propulsion force in the latest decades. A variety of theoretical studies have been shown in the existing literatures, such as the fuzzy logic control theory [5], the course keeping control [6], the reactive path planning [7], etc. In [8], the fuzzy control system is presented based on the three degrees of freedom (3-DOF) mathematical model. The sailboat can automatically achieve sailing along with desired course, except for the upwind or downwind conditions. Since the rolling dynamic plays an vital role in the marine engineering, a nonlinear 4-DOF mathematical model for USR has been developed in [9,10]. Furthermore, a course-keeping control law was designed for a class of keeled sailboats based on the backstepping method. The global uniform asymptotic stability has been proved for the closed-loop control system [11]. Though the course-keeping control of USR is meaningful, it is not enough to execute the complex autonomous missions [12,13]. In [14], a straight-line path following algorithm was developed with the maximum sailing speed. The simulated experiment has been presented to verify the good performance of the algorithm. Though the straight line trajectory is the shortest between the two target points, that may be not achievable for the USR in some practical scenes, due to its dependence on the wind energy. Considering the multiple sailing scenarios, a computed method was presented in [15] to obtain the suitable route to reach any specified targets. That is to say, the USR can sail in the upwind, the downwind or the crosswind scenes, respectively. To further improve the effectiveness of the algorithm, a potential fields-based path planning approach was developed for the navigation module of USR [16]. In the algorithm, the sail angle was computed from the speed polar diagram, which presents the correlation chart between the steady-state maximum speed and the given wind speed/angle.

In the aforementioned studies, there exist three major problems to be discussed. The first one is about the sailing speed control of USR. Actually, in the existing literatures, several researchers dedicated to obtain the maximizing sailing speed by optimizing the sail angle [16]. In [4], an online speed optimization algorithm is developed by using the extreme seeking method. Furthermore, a modified velocity optimizer is proposed to eliminate the speed chattering affect in

[17]. Though the maximizing sailing speed is helpful for the autopilot of USR, the violent speed may cause the instability or invalidity of the closed-loop control system, even leads to the capsizing of the sailboat. Thus, it is significant to regulate the appropriate sailing speed for the path following task of the USR. Second, the actuators' gain uncertainties are the common constrains in the practical plant. They are assumed to be known in the aforementioned literatures. That does not meet the marine practice and may destroy the effectiveness and accuracy of the related theoretical algorithms. In authors' previous works [18,19], the constraints of actuators' gain uncertainties are tackled with the robust neural damping technique and the dynamic surface control (DSC). However, there are some differences between the unmanned sailboat robot and the conventional surface ship due to their propulsion kinetics mechanism. Especially, the forces/moments generated by the sail are complicated and not allegiant only to the propulsion effect of the ship hull. The third major problem is that the varying waypoint-based can change the apparent direction of wind for the USR, and lead to the wind propulsion decrease or loss. Therefore, the intelligent guidance principle desires to be targetly designed for the USR. In the works [20–23], the integral line of sight (ILOS) was incorporated with the stability theory of cascade interconnected system to set the desired heading angle ψ_{ILOS}. For the USR, the ILOS guidance principle can provide the reference signal in crosswind scenario. However, for the upwind or downwind scenarios, the ILOS law is invalid due to the zigzag route deviates from the reference path.

Motivated by the aforementioned observations, this note focuses on the design of the guidance and path following control system for the USR under the external disturbances. The main novelty of this design can be summarized as follows:

1. To implement the practical waypoints-based path following mission, a composite ILOS guidance principle is developed for USR, aiming to three guidance modes: the upwind case, the downwind case and the crosswind one. Especially for the automatic navigation capabilities to conditions of upwind and downwind, the proposal is meaningful and significant for improving the autonomous of USR.
2. Compared with the previous works [18,19], the robust fuzzy control algorithm is proposed for USR

to design the speed regulator and the heading controller, which can adjust the maximum speed to the desired speed and stabilize the heading angle ψ to the desired heading angle ψ_d. Last but not least, the proposed algorithm is with the characteristic of the concise form and the lower computational burden for merits of the DSC and the robust fuzzy damping methods [19].

2 Nonlinear dynamic model and function approximation

2.1 Nonlinear dynamic model of USR

By using the physical reasoning for the sailboat model [11], the 4-DOF nonlinear dynamic model of the USR in a vectorial form, considering the rolling motion, has been developed. Via the model translation, the mathematical model of the USR in the horizontal plane can be expressed as Eqs. (1) and (2).

$$\begin{cases} \dot{x} = u\cos(\psi) - v\cos(\phi)\sin(\psi) \\ \dot{y} = u\sin(\psi) + v\cos(\phi)\cos(\psi) \\ \dot{\phi} = p \\ \dot{\psi} = r\cos(\phi) \end{cases} \quad (1)$$

$$\begin{cases} \dot{u} = \frac{1}{m_u}(S_u + R_u + K_u + m_v vr - D_u) + d_{wu} \\ \dot{v} = \frac{1}{m_v}(S_v + R_v + K_v + m_u ur - D_v) + d_{wv} \\ \dot{p} = \frac{1}{m_p}(S_p + R_p + K_p - G(\phi) - D_p) + d_{wp} \\ \dot{r} = \frac{1}{m_r}(S_r + R_r + K_r - (m_v - m_u)uv - D_r) + d_{wr} \end{cases} \quad (2)$$

where $\boldsymbol{v} = [u, v, p, r]^{\mathrm{T}}$, $m_u = m - X_{\dot{u}}$, $m_v = m - Y_{\dot{v}}$, $m_p = I_x - K_{\dot{p}}$, $m_r = I_z - N_{\dot{r}}$. $G(\phi)$ represents the static righting moment, and can be described as $G(\phi) = mgGM_t \sin(\phi)\cos(\phi)$. Figure 1 displays the basic illustration of the sailboat and the definition of the n-frame and b-frame. The involved variable definitions in Eqs. (1)–(7) and Fig. 1 can be displayed in Table 1.

For the USR, the related actuating force and moment are the sail thrust S_u for the surge and the rudder turning moment R_r for the yaw motion. The other forces and moments generated by the sail, rudder, keel, hull can be deemed as the perturbation and structure uncertainties. Furthermore, the sail thrust S_u and the rudder turning moment R_r can be expressed as Eqs. (3) and (4).
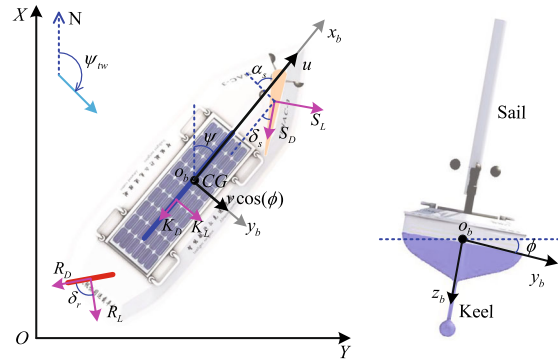

Fig. 1 Illustration of the n-frame and b-frame

$$S_u = \frac{1}{2}\rho_a A_s U_{aw}^2 C_{S_L}(\alpha_s)\,|\sin(\beta_{ws})| \quad (3)$$

$$R_r = \frac{1}{2}\rho_w A_r U_{ar}^2 C_{R_L}(\alpha_R)\,|x_r| \quad (4)$$

Furthermore, α_s and α_R can be described as Eq. (5).

$$\alpha_s = \beta_{ws} - \delta_s, \quad \alpha_R = \beta_{wr} - \delta_r \quad (5)$$

Note, considering the influence of the wake flow, it is reasonable to assume that $\beta_{wr} = 0$, which is also set in [11].

Remark 1 The lift coefficients $C_{S_L}(\alpha_s)$ and $C_{R_L}(\alpha_R)$ of the sail and rudder are related to the size, the shape, even the smoothness level of the corresponding facilities (the sail or the rudder). Actually, for a sailboat, $C_{S_L}(\alpha_s)$ and $C_{R_L}(\alpha_R)$ can be obtained from the sea-trial [11]. However, the data for $C_{S_L}(\alpha_s)$ and $C_{R_L}(\alpha_R)$ is with the form of discrete numerical point, see Fig. 2 (black numerical point). To facilitate the implementation of the control program, the data fitting technique is employed and the fitting effects can be shown in Fig. 2. Though the fitting error may be existed for the sailing ships, it can be stabilized for merits of the well robustness of the proposed controller. Thus, the fitting function can be expressed as Eq. (6).

$$\begin{aligned} C_{S_L}(\alpha_s) &= a_i(\beta_{ws} - \delta_s) + b_i \\ C_{R_L}(\alpha_R) &= \epsilon_1 \sin(-\epsilon_2 \delta_r) \end{aligned} \quad (6)$$

where a_i, b_i, ϵ_1, ϵ_2 are the fitting coefficients.

For a class of the keeled sailboat, the keel is applied to compensate the rolling force or moment, generated by the sail, rudder and hull. In addition, the lift force of the sail can be expressed as Eq. (7).

Table 1 The main symbols definition for USR

Indexes	Items
m	Mass of USR
g	Acceleration of gravity
CG	Center of gravity
OXY	Inertial reference frame (n-frame)
$o_b x_b y_b$	Body fixed frame (b-frame)
$X_{\dot{u}}, Y_{\dot{v}}\ K_{\dot{p}}\ N_{\dot{r}}$	Hydrodynamic derivatives in the surge, Sway, roll and yaw degree of freedom
I_x, I_z	Moment of inertia around surge/heave
GM_t	Transverse metacentric height
x, y	Surge, sway displacement in n-frame
ϕ, ψ	Rolling and heading angles in n-frame
u, v, p, r	Surge, sway, rolling and yaw velocities
d_{wu}, d_{wv}	Disturbing forces in surge and sway
d_{wp}, d_{wr}	Disturbing moments in roll and yaw
S_i, R_i, K_i, D_i	Forces/moments, generated by sail, Rudder, keel and hull in surge, sway, Roll and yaw, $i = u, v, p, r$
δ_r, δ_s	Rudder/sail angle in b-frame
S_L, S_D	Lift/drag force acting on sail
R_L, R_D	Lift/drag force acting on rudder
K_L, K_D	Lift/drag force acting on hull
A_s, A_r	Area of the sail and rudder
β_{ws}, β_{wr}	Relative wind/current angle
U_{aw}, U_{ar}	Relative wind/current speed
ψ_{tw}	True wind angle in n-frame
x_r	Rudder's centroid in b-frame
α_R, α_s	Attack angle of the rudder/sail
C_{S_L}, C_{R_L}	Lift coefficients of the sail/rudder
ρ_a, ρ_w	Air/water density

$$S_L = \frac{1}{2}\rho_a A_s U_{aw}^2 C_{S_L}(\alpha_s) \qquad (7)$$

Remark 2 The 4-DOF nonlinear dynamic mathematical model Eqs. (1) and (2) has been developed based on the four parts (i.e. the sail, rudder, keel and hull) in [11]. However, the external disturbances, caused by sea wind and sea wave, is not considered in literature [11]. That can affect the stability of closed-loop control system in the practical engineering. Hence, the external disturbances for the mathematical model have been taken into account in this note. That meets the practical marine engineering and can improve the reasonability of non-
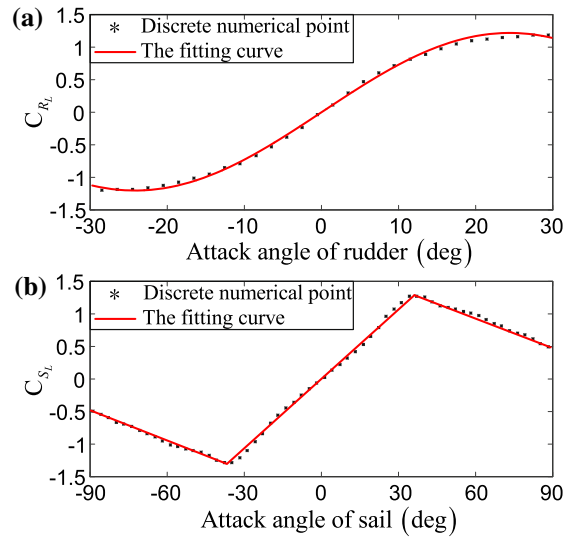
Fig. 2 The fitting effects of the rudder and sail coefficients by continuous functions

linear mathematical model. In addition, the true wind direction and speed can be measured by the anemometer. The heading angle and roll angle can be collected by the compass and clinometry. The position and the ship velocity can be obtained by the global positioning system (GPS). The forces or the moments generated by rudder, keel and hull can be calculated similar with the Eq. (7). Therefore, the 4-DOF nonlinear dynamic mathematical model is effective and considerate.

The objective of the note contains two points: (1) to present a composite ILOS guidance strategy which can guide the USR sail in the reference path, including the crosswind path, upwind path and downwind path. (2) to propose the robust fuzzy speed regulator and heading controller which can adjust the maximum speed to the desired speed and stabilize the heading angle ψ to the desired heading angle ψ_d.

To facilitate the discussions, the following assumptions are useful.

Assumption 1 The sway motion of the underactuated vehicles is passive bounded stable based on the results in [24]. It indicates that the sway speed of USR is bounded and the yaw motion is uniform ultimate bounded.

Assumption 2 For the nonzero external disturbance $d_{wi}, i = u, v, p, r$, there exists an unknown positive constants $\bar{d}_{wi}, i = u, v, p, r$, satisfied that $|d_{wi}| \le \bar{d}_{wi}$.

2.2 Function approximation via the fuzzy logic systems

In the control systems, radius based function neural networks and fuzzy logic systems (FLS) are frequently used as an valid tool for modeling nonlinear functions due to its merits in function approximation [25–27]. If FLS is employed, the fuzzy rule can be deduced as following:

If ς_1 is $L_1^{l_1}$, ς_2 is $L_2^{l_2}, \cdots, \varsigma_n$ is $L_n^{l_n}$, then h is $F^{l_1 \cdots l_n}$ where $[\varsigma_1, \varsigma_2, \cdots, \varsigma_n]^{\mathrm{T}} \in_\varsigma \subset \mathbb{R}^n$ is the input variable and $h \in_\varsigma$ is the output variable. $L_i^{l_i} (i = 1, 2, \cdots, n$ and $l_i = 1, 2, \cdots, s_i)$ and s_i are the fuzzy set and the number of the fuzzy set for the input variable ς_i, respectively. $F^{l_1 \cdots l_n} (l_1, l_2, \cdots l_n = 1, 2, \cdots, N, N = \prod_{i=1}^n s_i)$ and N are the fuzzy set for the output variable h and the total number of rules in the fuzzy rule. Based on the fuzzification, the fuzzy rule base and the defuzzification operators [28], the fuzzy logic system can be expressed as Eq. (8).

$$h(\varsigma) = \frac{\sum_{l=1}^N \bar{h}_l \prod_{i=1}^n \mu_{L_i^l}(\varsigma_i)}{\sum_{l=1}^N [\prod_{i=1}^n \mu_{L_i^l}(\varsigma_i)]} \tag{8}$$

where $\bar{h}_l = \max_{h_l \in \Re} \mu_{F^l}(h_l)$. Furthermore, the fuzzy basis functions can be defined as Eq. (9).

$$\theta_i^l(\varsigma_i) = \frac{\prod_{i=1}^n \mu_{L_i^l}(\varsigma_i)}{\sum_{l=1}^N (\prod_{i=1}^n \mu_{L_i^l}(\varsigma_i))} \tag{9}$$

The membership function of L_i^l is described as Eq. (10).

$$\mu_{L_i^l}(\varsigma_i) = \exp \frac{-(\varsigma_i - \varpi_i^l)^2}{2(z_i^l)^2} \tag{10}$$

where ϖ_i^l and z_i^l are the centers and widths of $\mu_{L_i^l}(\varsigma_i)$, respectively. Define

$$\begin{aligned} \theta(\varsigma) &= [\theta_1^l(\varsigma), \theta_2^l(\varsigma), \cdots, \theta_N^l(\varsigma)]^{\mathrm{T}} \\ \omega^* &= [\bar{h}_1, \bar{h}_2, \cdots, \bar{h}_N]^{\mathrm{T}} \end{aligned} \tag{11}$$

Then the fuzzy logic system (8) can be expressed as the linearization form:

$$h(\varsigma) = \omega^* \theta(\varsigma) \tag{12}$$

Lemma 1 (Nonlinear fuzzy approximation theorem [29]). *For arbitrary given continuous function $L(\varsigma) \in_\varsigma \subset \mathbb{R}$ with $L(0) = 0$, can be approximated by fuzzy logic system (12). It can be written as Eq. (13).*

$$\sup_{\varsigma \in_\varsigma} |L(\varsigma) - \omega^* \theta(\varsigma)| \leq \varepsilon \tag{13}$$

where ε is random positive error constant, satisfies $|\varepsilon| \leq \bar{\varepsilon}$, where $\bar{\varepsilon} > 0$ is unknown bounded.

3 Composite ILOS guidance for USR

The waypoints-based automatic navigation of USR is very significant in the engineering practice for that the operator often design the planned route by setting the waypoints. In the proposed guidance principle, the parameterized reference path is often generated by the waypoints-based path $W_1, W_2, \cdots, W_n$ with $W_i = (x_i, y_i), i = 1, 2, \cdots, n$. The ILOS guidance principle is usually applied to implement the path following control for the common marine vessel. However, the single ILOS guidance principle maybe inapplicable to upwind and downwind sailing for the USR.

Remark 3 Being different from the traditional marine surface vessels, the surge thrust is provided by the sail rather than propellers. Due to the sail is greatly influenced by the wind direction, not all the reference waypoints-based path are navigable. For the scenarios of upwind and downwind, the traditional controller is invalid. Therefore, the navigated zone should be divided into three zones, i.e., the upwind zone, the crosswind zone and the downwind zone. Figure 3 describes the relation between the course and the wind direction for the USR. Figure 3b, d is the crosswind zone, where the USR can navigate normally. Figure 3a is the upwind zone, where the USR cannot navigate. Figure 3c is the downwind zone, where the USR can navigate inefficiently. These restrictions have to be took into account in marine practical engineering. To avoid these restrictions and reach any specific target autonomously, a zigzag route is considered in upwind or downwind zones.

Therefore, to guide the USR toward a desired path generated by waypoints, the composite ILOS guidance in this section can be analyzed from three components: the crosswind sailing guidance (see Fig. 4b), the upwind sailing guidance (see Fig. 4a) and the downwind sailing guidance (see Fig. 4c).
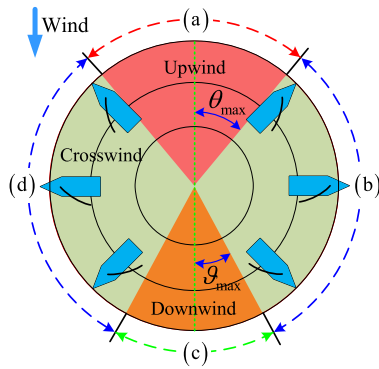
Fig. 3 Zones of sail: **a** upwind zone; **b**, **d** crosswind zone; **c** downwind zone
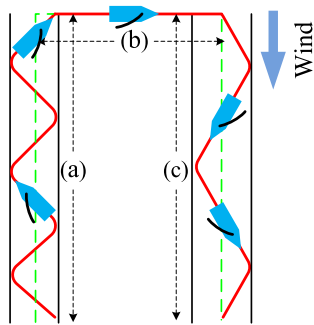

Fig. 4 Three guidance mode

3.1 Crosswind sailing guidance

As is described in Fig. 5, the parameterized path is generated by waypoints. η indicates the path variable and the inertial reference position is indicated by $(x_r(\eta), y_r(\eta))$ with random given η. The path tangential angle $\psi_r(\eta)$ is derived by $\psi_r(\eta) = \arctan 2(y_r', x_r')$ with $x_r' = \mathrm{d}x_r/\mathrm{d}\eta$, $y_r' = \mathrm{d}y_r/\mathrm{d}\eta$. As for the present position of the USR is indicated by (x, y) and the along-track error x_e and the cross-track error y_e along with the reference path can be expressed by Eq. (14).

$$\begin{bmatrix} x_e \\ y_e \end{bmatrix} = \begin{bmatrix} \cos(\psi_r) & \sin(\psi_r) & 0 \\ -\sin(\psi_r) & \cos(\psi_r) & 0 \end{bmatrix} \begin{bmatrix} x - x_r(\eta) \\ y - y_r(\eta) \end{bmatrix} \quad (14)$$

Time derivative of x_e, y_e can be written as Eq. (15).

$$\begin{cases} \dot{x}_e = (\dot{x} - \dot{x}_r)\cos(\psi_r) + (\dot{y} - \dot{y}_r)\sin(\psi_r) + \dot{\psi}_r y_e \\ \dot{y}_e = -(\dot{x} - \dot{x}_r)\sin(\psi_r) + (\dot{y} - \dot{y}_r)\cos(\psi_r) - \dot{\psi}_r x_e \end{cases} \quad (15)$$
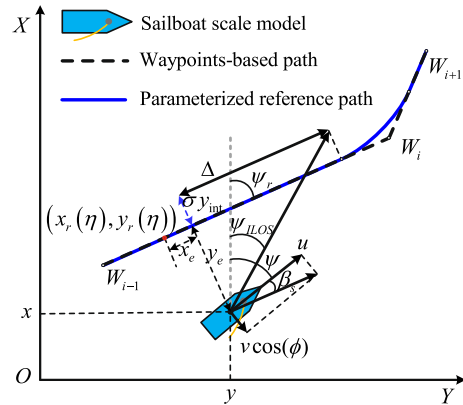

Fig. 5 Parameterized path framework of ILOS guidance law

Submitting Eq. (1) into Eq. (15), it follows that:

$$\begin{cases} \dot{x}_e = u\cos(\psi - \psi_r) - v\sin(\psi - \psi_r) + \dot{\psi}_r y_e - u_d \\ \dot{y}_e = U\sin(\psi - \psi_r + \beta_s) - \dot{\psi}_r x_e \end{cases} \quad (16)$$

where $U = \sqrt{u^2 + (v\cos(\phi))^2}$ indicates the velocity of the USR, $\beta_s = \arctan 2(v\cos\phi, u)$ describes the sideslip angle [30], see Fig. 5, and the virtual reference velocity u_d can be described as Eq. (17).

$$u_d = \dot{\eta}\sqrt{x_r'^2 + y_r'^2} \quad (17)$$

Furthermore, the ILOS guidance law is derived as Eq. (18).

$$\psi_{\mathrm{ILOS}} = \psi_r - \arctan\left(\frac{y_e + \sigma y_{\mathrm{int}}}{\Delta}\right) - \beta_s \quad (18)$$

$$\dot{y}_{\mathrm{int}} = \frac{\Delta y_e}{(y_e + \sigma y_{\mathrm{int}})^2 + \Delta^2} \quad (19)$$

where ψ_{ILOS} is the desired heading angle in the crosswind case. Δ is the look-ahead distance and σ is the integral gain [31]. Both are positive design parameters. ψ_{ILOS} can be further expressed as Eq. (20).

$$\psi_d = \psi_{\mathrm{ILOS}} \quad (20)$$

For the Eq. (16), u_d is the speed of the virtual reference point. To stabilize the along-track error x_e, u_d can be devised as Eq. (21).

$$u_d = \begin{cases} u_{d0}, & u_{d0} \le u_d^\star \\ u_d^\star, & u_{d0} > u_d^\star \end{cases} \tag{21}$$
$$u_{d0} = U \cos(\psi - \psi_r + \beta_s) + k_x x_e$$

where k_x is a positive constant parameter and $u_d^\star$ denotes the desired speed.

From Eqs. (17) and (21), the update law for the path variable is described as Eq. (22).

$$\dot{\eta} = \frac{u_d}{\sqrt{x_r'^2 + y_r'^2}} \tag{22}$$

Substituting Eq. (21) into the Eq. (16), Eq. (23) can be derived.

$$\begin{cases} \dot{x}_e = -k_x x_e + \dot{\psi}_r y_e \\ \dot{y}_e = U \sin(\psi - \psi_r + \beta_s) - \dot{\psi}_r x_e \end{cases} \tag{23}$$

3.2 Upwind and downwind sailing guidance

As is defined by upwind zone, the heading angle ψ locates in the upwind zone, see Fig. 3. The upwind angle related to true wind angle ψ_{tw} can be described by $|\psi_{tw} - \pi \operatorname{sgn}(\psi_{tw}) - \psi_{\text{ILOS}}| < \theta_{\max}$, and $\theta_{\max}$ is the boundary of upwind zone. In this mode, the USR will sail along with a zigzag path and tacking automatically with a definite distance constraint, see Fig. 4a. Furthermore, a sign function $\zeta(t)$ is defined to achieve the tacking maneuvering. $\zeta(t)$ is expressed as Eq. (24).

$$\zeta(t) = \operatorname{sgn}(y_e(t) + d_{c1}\operatorname{sgn}(\zeta(t-1))) \tag{24}$$

where d_{c1} denotes the distance constraint for upwind sailing. From the Eq. (24), $\zeta(t)$ will change its sign automatically if $|y_e| \ge d_{c1}$. Therefore, the desired heading angle ψ_d can be expressed as Eq. (25).

$$\psi_d = \psi_{tw} - \pi \operatorname{sgn}(\psi_{tw}) - \zeta(t)\theta_{\max} - \beta_s \tag{25}$$

As is defined by downwind mode, the heading angle ψ locates in the downwind zone, see Fig. 3. The downwind angle related to the true wind angle ψ_{tw} can be describe by $|\psi_{tw} - \psi_{\text{ILOS}}| < \vartheta_{\max}$, and $\vartheta_{\max}$ is the boundary of downwind zone. To obtain the optimizing speed and decrease the sailing time of the USR, a zigzag path with a certain distance constraint is necessary, see Fig. 4c. Analogous to the upwind mode, the sign function $\zeta(t)$ is expressed as Eq. (26).

$$\zeta(t) = \operatorname{sgn}(y_e(t) + d_{c2}\operatorname{sgn}(\zeta(t-1))) \tag{26}$$

where d_{c2} denotes the distance constraint for downwind sailing. Therefore, the desired heading angle ψ_d can be expressed as Eq. (27).

$$\psi_d = \psi_{tw} - \zeta(t)\vartheta_{\max} - \beta_s \tag{27}$$

4 Robust fuzzy speed regulator and heading controller

In this section, the fuzzy adaptive speed regulator and heading controller were designed for the system (1) and (2) by employing the FLS and DSC technique. From the dynamic errors (14) and the mathematical model (1) and (2), the errors dynamic derivatives and the simply nonlinear system can be derived as Eq. (28).

$$\begin{cases} \dot{x}_e = u \cos(\psi - \psi_r) - v \sin(\psi - \psi_r) + \dot{\psi}_r y_e - u_d \\ \dot{y}_e = u \sin(\psi - \psi_r) + v \cos(\psi - \psi_r) - \dot{\psi}_r x_e \\ \dot{\psi}_e = \dot{\psi} - \dot{\psi}_d \end{cases} \tag{28}$$

$$\begin{cases} \dot{\psi} = r \cos(\phi) \\ \dot{u} = \frac{m_v}{m_u}vr - \frac{f_u(\mathbf{v})}{m_u} + \frac{g_u}{m_u}C_{S_L}(\alpha_s) + d_{wu} \\ \dot{r} = \frac{m_u - m_v}{m_r}uv - \frac{f_r(\mathbf{v})}{m_r} + \frac{g_r}{m_r}C_{R_L}(\alpha_R) + d_{wr} \end{cases} \tag{29}$$

with

$$\begin{aligned} g_u &= \frac{1}{2}\rho_a A_s U_{aw}^2 |\sin(\beta_{ws})| \\ g_r &= \frac{1}{2}\rho_w A_r U_{ar}^2 |x_r| \end{aligned} \tag{30}$$

where $f_u(\mathbf{v})$ and $f_r(\mathbf{v})$ are the nonlinear terms of the closed-loop control system.

Remark 4 In Eq. (30), the function g_r can satisfy that $g_r > 0$ due to the variables ρ_w, A_r, U_{ar}^2, $|x_r|$ are the positive. In addition, the apparent wind angle β_{ws} satisfies the Eq. (31) for merits of the robust fuzzy speed regulator and can avoid the case of $\beta_{ws} = 0$ in the closed-loop control system. Thus, the function g_u also satisfies $g_u > 0$.

$$\beta_{ws} = \begin{cases} \theta_{\max}, & 0 \le \beta_{ws} \le \theta_{\max} \\ \beta_{ws}, & \theta_{\max} < \beta_{ws} \le \pi - \vartheta_{\max} \\ \pi - \vartheta_{\max}, & \pi - \vartheta_{\max} < \beta_{ws} \le \vartheta_{\max} \\ \pi + \vartheta_{\max}, & \pi < \beta_{ws} \le \pi + \vartheta_{\max} \\ \beta_{ws}, & \pi + \vartheta_{\max} < \beta_{ws} \le 2\pi - \theta_{\max} \\ 2\pi - \theta_{\max}, & 2\pi - \theta_{\max} < \beta_{ws} < 2\pi \end{cases}$$
(31)

4.1 Control design

Step 1. At this step, to stabilize the error dynamic (28), one defines the error variables $u_e = \alpha_u - u$, $r_e = \alpha_r - r$. The virtual controllers α_u and α_r can be defined as Eq. (32).

$$\alpha_u = (-k_x x_e + u_d)\frac{1}{\cos(\psi_{r\text{sat}})}$$
$$\alpha_r = \frac{1}{\cos(\phi)}(-k_r \psi_e + \dot{\psi}_d)$$
(32)

where $\psi_{r\text{sat}}$ is the saturation variable, k_x and k_r are the positive design parameters. The differential of the α_u and α_r is difficult to obtain and may cause the so called "explosion of complexity" in the next control design. To evade the restriction, the derivative can be acquired through the DSC technique [32] and the command filter [33,34]. One lets the α_u and α_r pass through the first-order filters β_u, β_r with the time constants τ_u and τ_r, i.e.,

$$\tau_u \dot{\beta}_u + \beta_u = \alpha_u, \ \beta_u(0) = \alpha_u(0), \ q_u = \beta_u - \alpha_u$$
$$\tau_r \dot{\beta}_r + \beta_r = \alpha_r, \ \beta_r(0) = \alpha_r(0), \ q_r = \beta_r - \alpha_r \quad (33)$$

where the q_u and q_r are the errors of dynamic surface, and the time derivative can be derived as Eq. (34).

$$\dot{q}_u = \dot{\beta}_u - \dot{\alpha}_u$$
$$= -\frac{q_u}{\tau_u} + \frac{\partial \alpha_u}{\partial x}\dot{x} + \frac{\partial \alpha_u}{\partial y}\dot{y} + \frac{\partial \alpha_u}{\partial x_r}\dot{x}_r + \frac{\partial \alpha_u}{\partial y_r}\dot{y}_r$$
$$+ \frac{\partial \alpha_u}{\partial \psi}\dot{\psi} + \frac{\partial \alpha_u}{\partial \psi_{r\text{sat}}}\dot{\psi}_{r\text{sat}} + \frac{\partial \alpha_u}{\partial u_d}\dot{u}_d$$
$$= -\frac{q_u}{\tau_u} + A_u$$
$$\dot{q}_r = -\frac{q_r}{\tau_r} + A_r$$
(34)

where A_u and A_r are the bounded continuous function and exist the positive constant M_u, M_r, satisfy

$|A_u| \le M_u$, $|A_r| \le M_r$. The detailed description can be referred to [19].

Remark 5 As for the possible singularity of the virtual control law α_u in Eq. (32), we define the saturation variable $\psi_{r\text{sat}}$ to ensure $|\psi - \psi_r| < 0.5\pi$. Furthermore, the heel angle ϕ can be small and satisfied $\phi \in (-0.5\pi, 0.5\pi)$ in the practical engineering. Thus, the possible singularity issue of the α_r can also be avoided.

$$\psi_{r\text{sat}} = \begin{cases} 0.5\pi - \ell, & \psi - \psi_r \ge 0.5\pi \\ \psi - \psi_r, & -0.5\pi < \psi - \psi_r < 0.5\pi \\ -0.5\pi + \ell, & \psi - \psi_r \le -0.5\pi \end{cases}$$
(35)

where ℓ is the positive small value, it is introduced to ensure the $\psi_{r\text{sat}} \in (-0.5\pi, 0.5\pi)$.

Step 2. At this step, one can define the intermediate control variables $u_{\delta_r} = C_{R_L}(\alpha_R)$, $u_{\delta_s} = C_{S_L}(\alpha_s)$. Thus, one can obtain the following error dynamic (36).

$$\dot{u}_e = \frac{1}{m_u}\left[m_u \dot{\beta}_u - m_v vr + f_u(\boldsymbol{v}) - g_u u_{\delta_s} - m_u d_{wu}\right]$$
$$\dot{r}_e = \frac{1}{m_r}\left[m_r \dot{\beta}_r - (m_u - m_v)uv + f_r(\boldsymbol{v}) - g_r u_{\delta_r} - m_r d_{wr}\right]$$
(36)

By the Lemma 1, $f_i(\boldsymbol{v})$, $i = u$, r can be approximated by the fuzzy logic system as Eq. (37).

$$f_i = \boldsymbol{\omega}_i^{*\text{T}}\boldsymbol{\theta}_i(\boldsymbol{v}) + \varepsilon_i$$
(37)

where the ε_i, $i = u, r$ are the arbitrary approximated errors. Then, one can construct the robust fuzzy damping term v_i, $i = u, r$. Benefiting from the robust fuzzy damping technique, the weights parameters information of the FLS is not needed. It brings great convenience for the control design. The $\|v_i\|_2$ can be expressed as Eq. (38) based on basic property of inequalities.

$$\|v_u\|_2 = \|\boldsymbol{\omega}_u^{*\text{T}}\boldsymbol{\theta}_u(\boldsymbol{v}) - m_v vr + \varepsilon_u - m_u d_{wu}\|_2$$
$$\le \|\boldsymbol{\omega}_u^{*\text{T}}\boldsymbol{\theta}_u(\boldsymbol{v}) + d_u \xi_u(\boldsymbol{v}) + \bar{\varepsilon}_u + m_u \bar{d}_{wu}\|_2$$
$$\le \vartheta_u \varphi_u$$
$$\|v_r\|_2 \le \vartheta_r \varphi_r$$
(38)

where the unknown upper bound parameter ϑ_i, $i = u$, r and the damping term φ_i, $i = u$, r can be described as Eq. (39).

$$
\begin{aligned}
\vartheta_i &= \max\{\|\boldsymbol{\omega}_i^{*\mathrm{T}}\|_2, d_i, \bar{\varepsilon}_i + m_i \bar{d}_{wi}\} \\
\varphi_i &= 1 + \|\xi_i(\boldsymbol{\nu})\|_2 + \|\boldsymbol{\theta}_i(\boldsymbol{\nu})\|_2 \\
\xi_u(\boldsymbol{\nu}) &= \frac{v^2}{4} + r^2, \ \xi_r(\boldsymbol{\nu}) = \frac{u^2}{4} + v^2
\end{aligned}
\tag{39}
$$

where d_i, $i = u$, r are the unknown positive constant.

Based to the above analysis, the error dynamic (36) can be rewritten as Eq. (40).

$$
\begin{aligned}
\dot{u}_e &= \frac{1}{m_u}\left[m_u\dot{\beta}_u + v_u - g_u u_{\delta_s}\right] \\
\dot{r}_e &= \frac{1}{m_r}\left[m_r\dot{\beta}_r + v_r - g_r u_{\delta_r}\right]
\end{aligned}
\tag{40}
$$

In the proposed algorithm, one employs the $\hat{\lambda}_{g_u}$, $\hat{\lambda}_{g_u}$ as the estimation of $\lambda_{g_u} = \frac{1}{g_u}$, $\lambda_{g_r} = \frac{1}{g_r}$. Hence, the singularities g_u and g_r can be avoided. They are two learning parameters which are turned online to compensate uncertainties of the system gain functions. The proposed algorithm aims to the control inputs δ_s and δ_r. The control laws and the corresponding adaptive laws are presented in Eqs. (41) and (42). In addition, the detailed theoretical analysis will be provided in the next section.

$$
\begin{aligned}
\delta_s &= \beta_{ws} - \frac{1}{a_i}(u_{\delta_s} - b_i), \ \delta_r = \frac{1}{\epsilon_2}\arcsin\left(\frac{1}{\epsilon_1}u_{\delta_r}\right) \\
u_{\delta_s} &= \hat{\lambda}_{g_u}\alpha_N, \ u_{\delta_r} = \hat{\lambda}_{g_r}\alpha_M \\
\alpha_N &= k_2 u_e + \dot{\beta}_u + \frac{1}{4}k_{un}\varphi_u^2 u_e - x_e\cos(\psi - \psi_r) \\
\alpha_M &= k_3 r_e + \dot{\beta}_r + \frac{1}{4}k_{rn}\varphi_r^2 r_e - \psi_e\cos(\phi) \\
\dot{\hat{\lambda}}_{g_u} &= \Gamma_{g_u}[\alpha_N u_e - \sigma_u(\hat{\lambda}_{g_u} - \hat{\lambda}_{g_u}(0))] \\
\dot{\hat{\lambda}}_{g_r} &= \Gamma_{g_r}[\alpha_M r_e - \sigma_r(\hat{\lambda}_{g_r} - \hat{\lambda}_{g_r}(0))]
\end{aligned}
\tag{41}
$$

$$
\tag{42}
$$

where k_2, k_3, k_{un}, k_{rn} denote the positive control parameters and Γ_{g_u}, σ_u, Γ_{g_r}, σ_r indicate the positive adaptive parameters.

4.2 Stability analysis

According to the aforementioned control design, the stability analysis of the closed-loop system is carried out in this section. The main result can be summarized as Theorem 1.

Theorem 1 *Consider the closed-loop system composed of the unmanned sailboat robot (1) and (2) meeting the assumption 1–2, the virtual control law (32), the fuzzy control law (41) and adaptive law (42). All the initial conditions satisfy $x_e^2(0) + y_e^2(0) + \psi_e^2(0) + u_e^2(0) + r_e^2(0) + q_u^2(0) + q_r^2(0) + \tilde{\lambda}_{g_u}^{\mathrm{T}}(0)\Gamma_{g_u}^{-1}\tilde{\lambda}_{g_u}(0) + \tilde{\lambda}_{g_r}^{\mathrm{T}}(0)\Gamma_{g_r}^{-1}\tilde{\lambda}_{g_r}(0) < 2C_0$ with any positive constant C_0. Then, one can guarantee that all the signals in the closed-loop system are SGUUB stability through turning the control parameters k_x, k_r, k_2, k_3, k_{un}, k_{rn}, Γ_{g_u}, σ_u, Γ_{g_r}, σ_r.*

Proof Based on the control design process, the Lyapunov function candidate is constructed as Eq. (43).

$$
\begin{aligned}
V &= \frac{1}{2}x_e^2 + \frac{1}{2}y_e^2 + \frac{1}{2}\psi_e^2 + \frac{1}{2}m_u u_e^2 + \frac{1}{2}m_r r_e^2 \\
&\quad + \frac{1}{2}q_u^2 + \frac{1}{2}q_r^2 + \frac{1}{2}\frac{g_u}{\Gamma_{g_u}}\tilde{\lambda}_{g_u}^2 + \frac{1}{2}\frac{g_r}{\Gamma_{g_r}}\tilde{\lambda}_{g_r}^2
\end{aligned}
\tag{43}
$$

Using the Eqs. (23), (40), the time derivative $\dot{V}$ can be derived as Eq. (44).

$$
\begin{aligned}
\dot{V} &= x_e\dot{x}_e + y_e\dot{y}_e + \psi_e\dot{\psi}_e + m_u u_e\dot{u}_e + m_r r_e\dot{r}_e \\
&\quad + q_u\dot{q}_u + q_r\dot{q}_r + \frac{g_u}{\Gamma_{g_u}}\tilde{\lambda}_{g_u}\dot{\tilde{\lambda}}_{g_u} + \frac{g_r}{\Gamma_{g_r}}\tilde{\lambda}_{g_r}\dot{\tilde{\lambda}}_{g_r} \\
&= x_e\left(-k_x x_e + \dot{\psi}_r y_e\right) - y_e\left(U\sin(\psi - \psi_r + \beta)\right. \\
&\quad \left. -\dot{\psi}_r x_e\right) + \psi_e\left(-k_{\psi_e}\psi_e - r_e\cos(\phi)\right) \\
&\quad + u_e\left[m_u\dot{\beta}_u - v_u - g_u u_{\delta_s}\right] + q_u\dot{q}_u \\
&\quad + r_e\left[m_r\dot{\beta}_r - v_r - g_r u_{\delta_r}\right] + q_r\dot{q}_r \\
&\quad - \frac{g_u}{\Gamma_{g_u}}\tilde{\lambda}_{g_u}\dot{\hat{\lambda}}_{g_u} - \frac{g_r}{\Gamma_{g_r}}\tilde{\lambda}_{g_r}\dot{\hat{\lambda}}_{g_r}
\end{aligned}
\tag{44}
$$

Noting that, from the trigonometric function transformation and Young's inequality, the following Eqs. (45)–(48) can be derived by fusing the robust fuzzy damping technique and be employed in the further derivation, $i = u$, r.

$$
\begin{aligned}
&\sin\left(\psi - \psi_{ILOS} - \arctan\left(\frac{y_e + \sigma y_{\text{int}}}{\Delta}\right)\right) \\
&= \frac{\Delta}{\sqrt{(y_e + \sigma y_{\text{int}})^2 + \Delta^2}}\sin(\psi_e)
\end{aligned}
$$

$$- \frac{\Delta}{\sqrt{(y_e + \sigma y_{\text{int}})^2 + \Delta^2}} \cos(\psi_e) \qquad (45)$$

$$\upsilon_i i_e = \vartheta_i \varphi_i i_e \leq \frac{k_{in}}{4} \varphi_i^2 i_e^2 + \frac{\vartheta_i^2}{k_{in}} \qquad (46)$$

$$m_i \dot{\beta}_i i_e - \dot{\beta}_i i_e \leq \frac{m_i + 1}{4} q_i^2 + \frac{m_i + 1}{\tau_i} i_e^2 \qquad (47)$$

$$q_i \dot{q}_i = -\frac{q_i^2}{\tau_i} - q_i \dot{\alpha}_i = -\frac{q_i^2}{\tau_i} - q_i A_i$$

$$\leq -\frac{q_i^2}{\tau_i} + \frac{q_i^2 A_i^2 M_i^2}{2a M_i^2} + \frac{a}{2}$$

$$\leq -\left(\frac{1}{\tau_i} - \frac{M_i^2}{2a}\right) q_i^2 - \left(1 - \frac{A_i^2}{M_i^2}\right) \frac{M_i^2 q_i^2}{2a} + \frac{a}{2}$$

$$\leq -\left(\frac{1}{\tau_i} - \frac{M_i^2}{2a}\right) q_i^2 + \frac{a}{2} \qquad (48)$$

Based on the control law (41), adaptive law (42) and Eqs. (45)–(48), the Eq. (44) can be further formulated as Eq. (49).

$$\dot{V} \leq - k_x x_e^2 - k_y y_e^2 - k_r \psi_e^2 - \left(k_2 - \frac{m_u + 1}{\tau_u}\right) u_e^2$$

$$- \left(k_3 - \frac{m_r + 1}{\tau_r}\right) r_e^2 - \left(\frac{1}{\tau_u} - \frac{M_u^2}{2a} - \frac{m_u + 1}{4}\right) q_u^2$$

$$- \left(\frac{1}{\tau_r} - \frac{M_r^2}{2a} - \frac{m_r + 1}{4}\right) q_r^2 - \sigma_u \Gamma_{g_u} \frac{g_u}{\Gamma_{g_u}} \tilde{\lambda}_{g_u}^2$$

$$- \sigma_r \Gamma_{g_r} \frac{g_r}{\Gamma_{g_r}} \tilde{\lambda}_{g_r}^2 + \frac{\vartheta_u^2}{k_{un}} + \frac{\vartheta_r^2}{k_{rn}} + U_{\max} y_e + a$$

$$- v x_e \sin(\psi - \psi_r) - \sigma_u g_u \tilde{\lambda}_{g_u} \left(\lambda_{g_u} - \hat{\lambda}_{g_u}(0)\right)$$

$$- \sigma_r g_r \tilde{\lambda}_{g_r} \left(\lambda_{g_r} - \hat{\lambda}_{g_r}(0)\right) \qquad (49)$$

where $U_{\max} = \min \left\{ U \Delta / \sqrt{(y_e + \sigma y_{\text{int}})^2 + \Delta^2} \right\}$, and $k_y = U_{\max}/\Delta$. Note that, the designed control parameters can be selected as follows. $k_2 = \gamma_1 + (m_u + 1)/\tau_u$, $k_3 = \gamma_2 + (m_r + 1)/\tau_r$, $\tau_u^{-1} = \gamma_3 + M_u^2/2a + (m_u + 1)/4$, $\tau_r^{-1} = \gamma_4 + M_r^2/2a + (m_r + 1)/4$. $\gamma_1, \gamma_2, \gamma_3$ and γ_4 are the positive constants. Thus, the Eq. (49) would be rewritten as Eq. (50).

$$\dot{V} \leq -2\kappa V + \varrho \qquad (50)$$

with

$$\kappa = \min \left\{ k_x, k_y, k_r, \gamma_1, \gamma_2, \gamma_3, \gamma_4, \sigma_u \Gamma_{g_u}, \sigma_r \Gamma_{g_r} \right\}$$

$$\varrho = \frac{\vartheta_u^2}{k_{un}} + \frac{\vartheta_r^2}{k_{rn}} + U_{\max} y_e - \sigma_u g_u \tilde{\lambda}_{g_u} \left(\lambda_{g_u} - \hat{\lambda}_{g_u}(0)\right)$$

$$- \sigma_r g_r \tilde{\lambda}_{g_r} \left(\lambda_{g_r} - \hat{\lambda}_{g_r}(0)\right) + a - v x_e \sin(\psi - \psi_r) \qquad (51)$$

One can get $V(t) \leq \varrho/2\kappa + (V(0) - \varrho/2\kappa) \exp(-2\kappa t)$ by integrating two sides of Eq. (50). The $V(t)$ can converge into $\varrho/2\kappa$ with $t \to \infty$, and the bounded variable ϱ can be small enough through turning the control parameters appropriately. Therefore, all the state variables in the closed-loop control system are SGUUB. The proof of Theorem 1 is completed. □

Remark 6 Compared with existing literatures, though the incorporated FLS is employed to tackle the system uncertainties, no FLS weights are required to update online for the superiority of the robust fuzzy damping technique. Besides, the selection of control parameters is a difficulty task on account of the parameters have coupling effect on system performance. Furthermore, the control orders are generated in real time to stabilize the output errors due to the time-varying external disturbances. That can cause the communication redundancy of the closed-loop control system.

5 Numerical simulation

In this section, two numerical simulations are developed to demonstrate the effectiveness of the proposed algorithm, consisting of the comparative experiment and the path following experiment in the field of external disturbances. For this purpose, the USR (length of $L = 12$m), equipped with one main sail, one rudder and one keel, is chosen as the plant, which has been employed in [10,11] as a standard sailboat. Though the control orders δ_r, δ_s are designed by the robust fuzzy damping technique and dynamic surface control, the control orders are needed to transmit to the rudder and the sail actuators by the servo system in the marine engineering. To deal with these engineering practice conditions, the results for the actual input δ_{ra}, δ_{sa} are provided in Sect. 5.2.
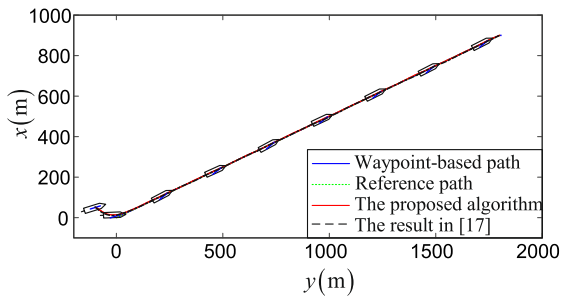
Fig. 6 Comparison of the path following trajectory

5.1 Comparative simulation

To verify the effectiveness and robustness of the proposed algorithm, the robust fuzzy speed regulator and heading controller are compared with the existing results [17]. In [17], the velocity optimizer, based on a modified extremum seeking approach, is presented to obtain the maximum velocity. For this purpose, the reference path is specified by two waypoints. $W_1(0m, 0m)$, $W_2(1800m, 900m)$, and the initial state variables are set as $[x(0), y(0), \phi(0), \psi(0), u(0), v(0), p(0), r(0), \delta_s(0), \delta_r(0)] = [-100m, 50m, 0deg, 0deg, 1m/s, 0m/s, 0deg/s, 0deg/s, 0deg, 0deg]$. The corresponding control parameters setting follows as Eq. (52). Note that, to obtain the satisfied system performance, we can try a few simulation runs and adjusting the parameters. In general, we can select small σ_u, σ_r and large $k_x, k_r, k_1, k_2, k_{un}, k_{rn}, \Gamma_{g_u}, \Gamma_{g_r}$. For the FLS, the centers for u, v, p, r are spaced in $[-5m/s, 15m/s] \times [-2.5m/s, 2.5m/s] \times [-1.5m/s, 1.5m/s] \times [-0.8m/s, 0.8m/s]$. For $f_u(\cdot), f_r(\cdot)$, the number of fuzzy rules are with the same setting $N = 21$.

$$\Delta = 15m, \ \sigma = 0.02, \ \theta_{max} = \pi/4, \ \vartheta = \pi/6,$$
$$d_{c1} = 40m, \ d_{c2} = 25m, \ k_x = 0.5, \ k_r = 0.6,$$
$$k_2 = 0.5, \ k_3 = 0.7, \ \Gamma_{g_u} = 1.02, \ \Gamma_{g_r} = 1.03,$$
$$\sigma_u = 0.05, \ \sigma_r = 0.03, \ \tau_u = 0.02, \ \tau_r = 0.02,$$
$$k_{un} = 0.2, \ k_{rn} = 0.3, \ \epsilon_1 = 1.191, \ \epsilon_2 = 3.678,$$
$$a_1 = 2.097, b_1 = 0.116, a_2 = -0.746, u_d^\star = 7,$$
$$b_2 = -1.759, \ a_3 = -1.744, \ b_3 = 1.752.$$
$$\tag{52}$$

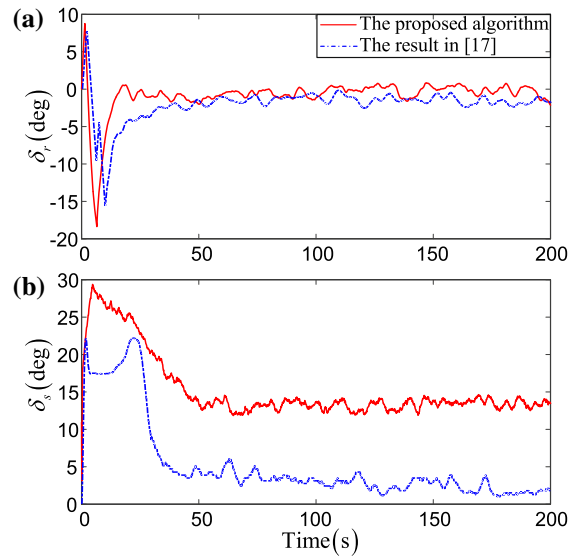Figures 6, 7, 8 and 9 present the main comparison results of the closed-loop system under the proposed

Fig. 7 Control inputs δ_r, δ_s: the proposed algorithm (red solid line) and the algorithm in [17] (blue dashed line)
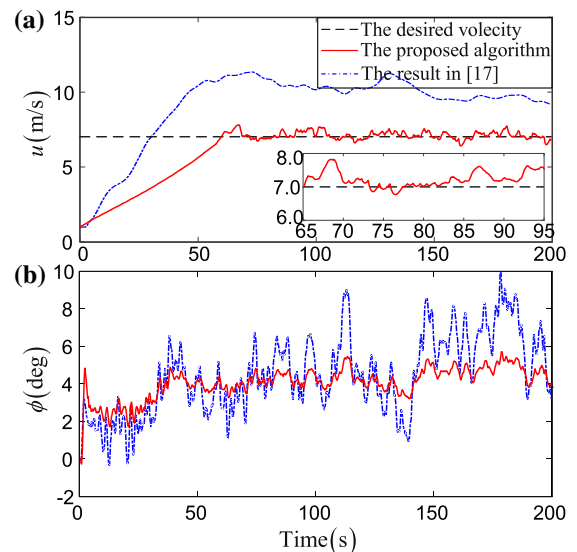

Fig. 8 Comparison of the kinematic variables under the both control algorithms

scheme and the existing results in [17]. Figure 6 shows the comparison trajectory of the straight-line path following under the two control algorithms. It is noted that the travel time of the proposed algorithm is 316.9s, and the one of the algorithm in [17] is 209.6s. For uniformity, only the previous 200s of the performance curves are presented in the Figs. 7, 8 and 9. One can obtain the control orders, and the kinematic variable u from the
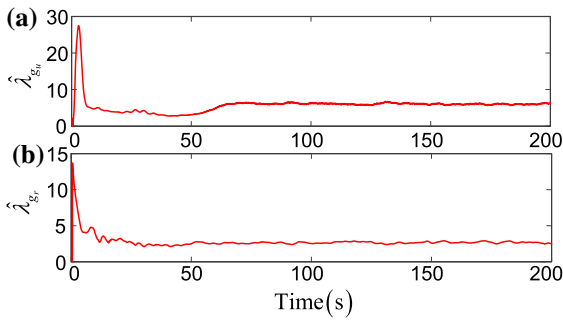
Fig. 9 Adaptive parameters $\hat{\lambda}_{g_u}$ and $\hat{\lambda}_{g_r}$ under the proposed algorithm

Table 2 Quantitative comparison of performances for the proposed algorithm and the result in [17]

Indexes	Items	The proposed algorithm	The result in [17]
MAS	u (m/s)	0.236	0.873
MAR	ϕ (deg)	4.384	5.893
	δ_r (deg)	0.216	2.013
MAI	δ_s (deg)	14.362	3.743
	δ_r (deg)	0.3021	0.3587
MTV	δ_s (deg)	<u>1.3751</u>	0.9694

Figs. 7 and 8. The rudder angle can be with the merits of convergence speed and energy consumption. The energy consumption of the sail structure is not only related to the sail angle, but also related to the sailing scenarios. That is related to the relative wind angle. Thus, though the sail angle in the proposed scheme (red solid line) is larger than the result in the existed literate (blue dashed line), the energy consumption of the proposed algorithm is smaller. The velocity of the USR can be converged to the desired objective by turning the sail angle under the robust fuzzy speed regulator. Figure 9 describes the variation of the adaptive parameters for the sail and rudder.

$$\text{MAS} = \frac{1}{t_{\text{end}} - 65} \int_{65}^{t_{\text{end}}} |u(t) - u_m| \ \mathrm{d}t$$
$$\text{MAR} = \frac{1}{t_{\text{end}} - 65} \int_{65}^{t_{\text{end}}} |\phi(t)| \ \mathrm{d}t$$
$$\text{MAI} = \frac{1}{t_{\text{end}} - 65} \int_{65}^{t_{\text{end}}} |\delta_i(t)| \ \mathrm{d}t, \quad i = r, s$$
$$\text{MTV} = \frac{1}{t_{\text{end}} - 65} \int_{65}^{t_{\text{end}}} |\delta_i(t+1) - \delta_i(t)| \ \mathrm{d}t$$

(53)

For the further quantitative comparison purpose, four popular performance specifications (53) are introduced to evaluate the compared algorithms, including the mean absolute speed performance (MAS), the mean absolute roll error (MAR), the mean absolute control input (MAI) and the mean total variation (MTV) of the control. The performance specifications are compared while the closed-loop system reaches the stability state, i.e., in 65s-200s. MAS can be utilized for measuring the speed response, u_{m} is the average speed. It was set as 7m/s and 10m/s for the proposed algorithm and the [17]. MAR is used for measuring the roll angle,

and it can describe the safety performance of system. MAI is utilized for measuring the properties of energy consumption, and MTV is utilized for measuring the properties of smoothness [19]. The related quantitative valuations of the simulations are measured and illustrated as Table 2. One can note that the speed can converge to the desired objective (7m/s) within a small deviation. Though the mean sail angle is 14.362deg in the proposed algorithm, the larger sail angle will generate the low thrust in this scenario and it may reduce the roll angle. That is significant to improve the safety of navigation. Thus, the proposed algorithm is with the superiority in aspects of the speed regulating and the system performance.

5.2 The path following simulation in the field of external disturbances

In this section, to demonstrate the effectiveness and robustness of the proposed algorithm, the numerical simulation achieves a waypoints-based guidance and control in presence of the complex path (including the upwind, downwind and crosswind conditions) under the simulated marine disturbances. For this purpose, the reference path consists of five waypoints: $W_1(0\text{m}, 0\text{m})$, $W_2(0\text{m}, 600\text{m})$, $W_3(1800\text{m}, 600\text{m})$, $W_4(1800\text{m}, 0\text{m})$ and $W_5(500\text{m}, 0\text{m})$. The conceptual signal flow box diagram for the closed-loop system is given in Fig. 10 and the marked numbers denote formulae involved in the corresponding box.

As to the external disturbances, the physical-based model in [35] are introduced. The NORSOK (The Competitive Standing of the Norwegian Offshore Sector) wind and the JONSWAP ((Joint North Sea Wave Observation Project) wave spectrums are adapted to
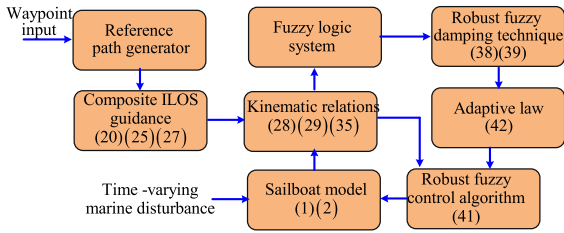
Fig. 10 Conceptual signal flow box diagram for the closed-loop system
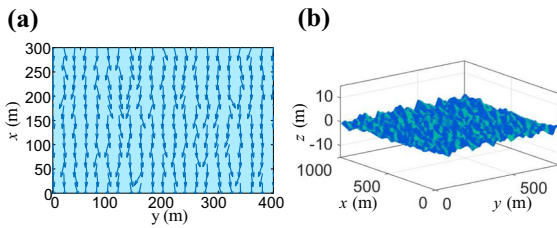

Fig. 11 External disturbances with the fifth level sea state. **a** The 2-D sketch field of sea wind. **b** The wind-generated waves.)
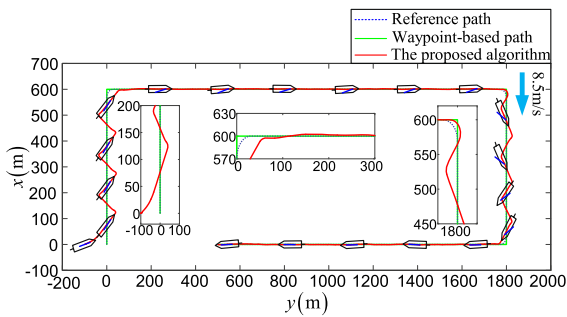

Fig. 12 The path following control trajectory for the proposed scheme

generate these simulated marine disturbances, i.e., the sea wind and the irregular wind-generated waves. The detailed deductive process of the wind and wave disturbances can be referred in [35]. Figure 11a describes the two-dimension slow time-varying wind field, and the main wind angle and the main wind speed are set as $\psi_{tw} = 0$deg, $U_{tw} = 8.5$m/s. The related wind-generated waves surface with the amplitude of fifth level sea state is illustrated in Fig. 11b. That is also set in Sect. 5.1.

Figures 12, 13, 14, 15 and 16 illustrate the main simulative results of the path following experiment in the external disturbances. From the Fig. 12, the green solid line indicates the waypoint-based path, the blue dashed line indicates the parameterized reference path
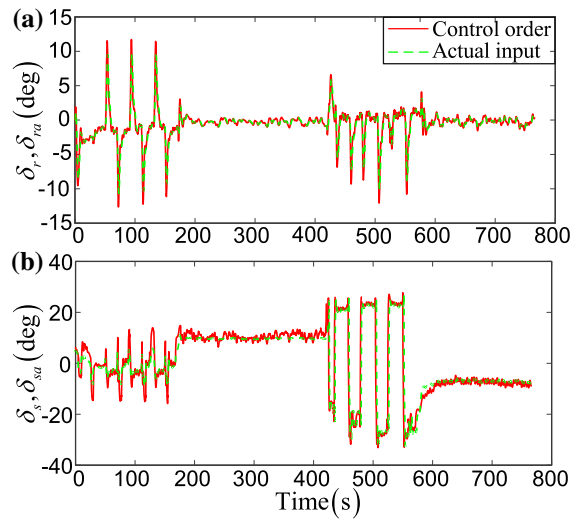
Fig. 13 Control inputs with composite ILOS guidance
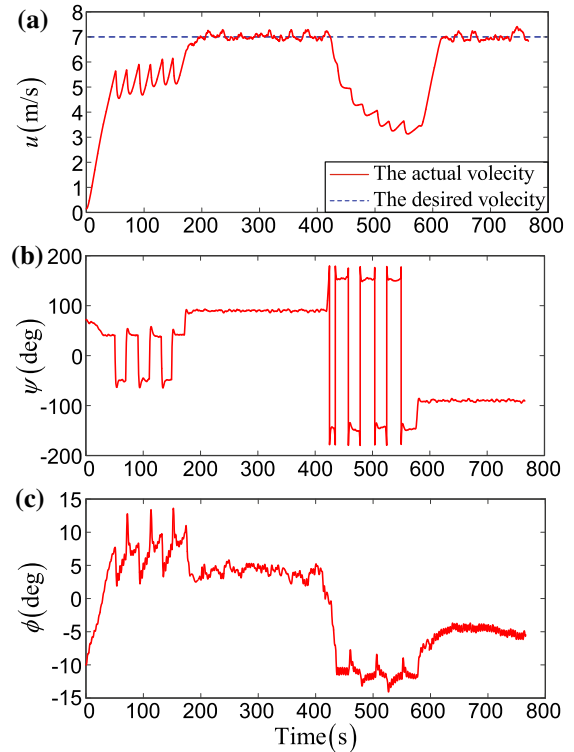
Fig. 14 Control outputs for the experiment under the proposed scheme

and the red solid line indicates the actual trajectory of the USR. In addition, the USR can effectively track the waypoint-based reference path by fusing the composite ILOS guidance principle and fuzzy adaptive con-
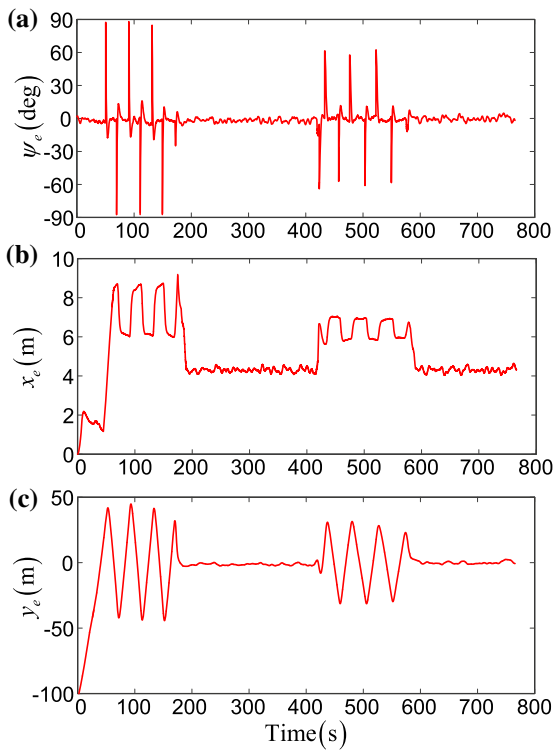
Fig. 15 Orientation and position errors for the proposed scheme
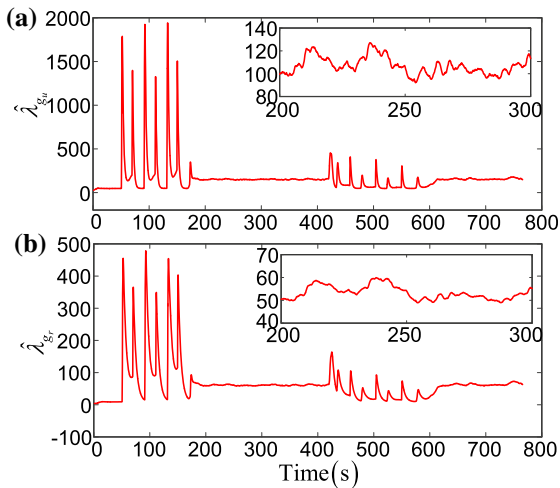

Fig. 16 Estimation of $\hat{\lambda}_{g_u}$ and $\hat{\lambda}_{g_r}$ for the proposed scheme

trol strategies. Especially, the upwind and downwind sailing guidance can achieve the zigzag trajectory and autoturn with the safety bandwidth restrictions when the USR sailing in the upwind and downwind conditions. Figure 13 presents the control order δ_r, δ_s (red

line) and the actual input δ_{ra}, δ_{sa} (green dashed line) of the experiment with the simulated external disturbances. It can be noted that the control orders are within the reasonable range for merits of the composite guidance and the robust fuzzy damping technique. Figure 14 describes the control outputs of the simulation experiment. It can be concluded that the kinematic variable u is with the good performance. While the USR sailing in the upwind and downwind scenes, the maximum velocity was generated by turning the sail. However, while sailing in the crosswind condition, the USR can successfully converge to the desired velocity by using the robust fuzzy speed regulator. The upwind and downwind scenes can strength the complexity and difficulty of the system, and this can be found in 50s–180s from the Figs. 15, 16. Based on the above analysis, the proposed composite ILOS law, robust fuzzy speed regulator and heading controller have a good performance in aspects of the path following and speed regulating. It is more in accordance with marine engineering requirements.

6 Conclusion

A novel robust fuzzy control algorithm has been developed to address the waypoints-based path following problem for USR by using the DSC and the robust fuzzy damping technique. The proposed scheme is capable to achieve the reasonable and effective regulation to the surge and the heading kinetics. It is concluded that the proposed algorithm is with the concise form, the performance of speed regulation and the small computation load, which can facilitate its applicability in the marine practice. Furthermore, the SGUUB stability of the closed-loop system has been proved through the Lyapunov criteria. From the comparative experiments, the proposed algorithm is effective, with the improved safety and robust performance. In the future work, the joint event-triggered control of USR using the sail, the rudder and the main propulsion system will be studied to further improve the effectiveness of the theoretical algorithm and its application in engineering practice.

References

1. Zhang, G., Li, J., Li, B., Zhang, X.: Improved integral LOS guidance and path-following control for an unmanned robot sailboat via the robust neural damping technique. J. Navig. **72**(6), 1378–1398 (2019)
2. Yeh ,E.C., Bin, J.-C.: Fuzzy control for self-steering of a sailboat. In: Proceedings of International Conference on Intelligent Control and Instrumentation (1992)
3. Cruz, N.A., Alves, J.C.: Autonomous sailboats: an emerging technology for ocean sampling and surveillance. In: Proceedings of the MTS-IEEE Conference Oceans (2008)
4. Xiao, L., Alves, J.C., Cruz, N.A., Jouffroy, J.: Online speed optimization for sailing yachts using extremum seeking. In: OCEANS 2012 MTS/IEEE: Harnessing the Power of the Ocean (2012)
5. Stelzer, R., Proll, T., John, R.: Fuzzy logic control system for autonomous sailboats. In: IEEE International Fuzzy Systems Conference (2007)
6. Tagliaferri, F., Viola, I.M.: A real-time strategy-decision program for sailing yacht races. Ocean Eng. **134**, 129–139 (2017)
7. Petres, C., Romero-Ramirez, M.A., Plumet, F., Alessandrini, B.: Modeling and reactive navigation of an autonomous sailboat. In: IEEE/RSJ International Conference on Intelligent Robots and Systems (2011)
8. Abril, J., Salom, J., Calvo, O.: Fuzzy control of a sailboat. Int. J. Approx. Reason. **16**(3–4), 359–375 (1997)
9. Deng, Y., Zhang, X., Zhang, G.: Line-of-sight-based guidance and adaptive neural path-following control for sailboats. IEEE J. Oceanic Eng. **45**(4), 1177–1189 (2020)
10. Wille, K.L., Hassani, V., Sprenger, F.: Modeling and course control of sailboats. Ifac Papersonline **49**(23), 532–539 (2016)
11. Xiao, L., Jouffroy, J.: Modeling and nonlinear heading control for sailing yachts. IEEE J. Oceanic Eng. **39**(2), 256–268 (2014)
12. Jaulin, L., Le Bars, F.: An interval approach for stability analysis: application to sailboat robotics. IEEE Trans. Rob. **29**(1), 282–287 (2013)
13. Tagliaferri, F., Philpott, A.B., Viola, I.M., Flay, R.G.J.: On risk attitude and optimal yacht racing tactics. Ocean Eng. **90**(90), 149–154 (2014)
14. Santos, D., Junior, A., Negreiros, A., Vilas Boas, J., Alvarez, J., Araujo, A., Aroca, R., Gonçalves, L.: Design and implementation of a control system for a sailboat robot. Robotics **5**, 5–28 (2016)
15. Stelzer, R., Proll, T.: Autonomous sailboat navigation for short course racing. Robot. Auton. Syst. **56**(7), 604–614 (2008)
16. Plumet, F., Petres, C., Romero-Ramirez, M.-A., Gas, B., Ieng, S.-H.: Toward an autonomous sailing boat. IEEE J. Oceanic Eng. **40**(2), 397–407 (2015)
17. Corno, M., Formentin, S., Savaresi, S.: Data-driven online speed optimization in autonomous sailboats. IEEE Trans. Intell. Transp. Syst. **17**(3), 1–10 (2015)
18. Zhang, G., Zhang, X., Zheng, Y.: Adaptive neural path-following control for underactuated ships in fields of marine practice. Ocean Eng. **104**, 558–567 (2015)
19. Zhang, G., Deng, Y., Zhang, W.: Robust neural path-following control for underactuated ships with the dvs obstacles avoidance guidance. Ocean Eng. **143**, 198–208 (2017)
20. Serrano, M.E., Scaglia, G., Godoy, S.A., Mut, V., Ortiz, O.A.: Trajectory tracking of underactuated surface vessels: a linear algebra approach. IEEE Trans. Control Syst. Technol. **22**(3), 1103–1111 (2014)
21. Xiang, X., Caoyang, Yu., Lapierre, L., Zhang, J., Zhang, Q.: Survey on fuzzy-logic-based guidance and control of marine surface vehicles and underwater vehicles. Int. J. Fuzzy Syst. **20**(2), 572–586 (2018)
22. Jin, X.: Adaptive fixed-time control for MIMO nonlinear systems with asymmetric output constraints using universal barrier functions. IEEE Trans. Autom. Control **64**(7), 3046–3053 (2019)
23. Huang, J., Wang, W., Xiaojie, S.: Adaptive iterative learning control of multiple autonomous vehicles with a time-varying reference under actuator faults. IEEE Trans. Neural Netw. Learn. Syst. (2021). https://doi.org/10.1109/TNNLS.2021.3069209
24. Do, K.D.: Practical control of underactuated ships. Ocean Eng. **37**(13), 1111–1119 (2010)
25. Li, Y., Tong, S.: Adaptive neural networks prescribed performance control design for switched interconnected uncertain nonlinear systems. IEEE Trans. Neural Netw. Learn. Syst. **29**(7), 3059–3068 (2018)
26. Li, D., Li, D., Liu, Y., Tong, S., Chen, C.L.P.: Approximation-based adaptive neural tracking control of nonlinear mimo unknown time-varying delay systems with full state constraints. IEEE Trans. Cybern. **47**(10), 3100–3109 (2017)
27. Wang, Y., Xie, X., Chadli, M., Xie, S., Peng, Y.: Sliding-mode control of fuzzy singularly perturbed descriptor systems. IEEE Trans. Fuzzy Syst. **29**(8), 2349–2360 (2021)
28. Bin, X., Wang, X., Shou, Y., Shi, P., Shi, Z.: Finite-time robust intelligent control of strict-feedback nonlinear systems with flight dynamics application. IEEE Trans. Neural Netw. Learn. Syst. (2021). https://doi.org/10.1109/TNNLS.2021.3072552
29. Li, Y., Tong, S.: Fuzzy adaptive control design strategy of nonlinear switched large-scale systems. IEEE Trans. Syst. Man Cybern. Syst. **48**(12), 2209–2218 (2018)
30. Zheng, Z., Liang, S., Xie, L.: Error-constrained los path following of a surface vessel with actuator saturation and faults. IEEE Trans. Syst. Man Cybern. Syst. **48**(10), 1794–1805 (2017)
31. Yang, Q., Cai, L., Haixiang, X.: Curved path following for unmanned surface vehicles with heading amendment. IEEE Trans. Syst. Man Cybern. Syst. **64**, 1–10 (2019)

32. Zhang, G., Li, J., Jin, X., Liu, C.: Robust adaptive neural control for wing-sail-assisted vehicle via the multiport event-triggered approach. IEEE Trans. Cybern. (2021). https://doi.org/10.1109/TCYB.2021.3091580

33. Vafamand, N.: Adaptive robust neural-network-based backstepping control of tethered satellites with additive stochastic noise. IEEE Trans. Aerosp. Electron. Syst. **56**(5), 3922–3930 (2020)

34. Homayoun, B., Arefi, M.M., Vafamand, N., Yin, S.: Neural minimal learning backstepping control of stochastic active suspension systems with hydraulic actuator saturation. J.Frankl. Inst. **357**(18), 13687–13706 (2020)

35. Mccue, L.: Handbook of marine craft hydrodynamics and motion control. IEEE Control. Syst. **36**(1), 78–79 (2016)